CHEMISTRY

Metal atom–guided conformational analysis of single polynuclear coordination molecules

Kenji Takada[1†], Mari Morita[1‡], Takane Imaoka[1,2*], Junko Kakinuma[1], Ken Albrecht[1,2*§], Kimihisa Yamamoto[1,2*]

Microscopic observation of single molecules is a rapidly expanding field in chemistry and differs from conventional characterization techniques that require a large number of molecules. One of such form of single-molecule microscopy is high-angle annular dark-field scanning transmission electron microscopy (HAADF-STEM), which is especially suitable for coordination compounds because of its atomic number–dependent contrast. However, to date, single-molecule observations using HAADF-STEM has limited to simple planar molecules. In the present study, we demonstrate a direct structural investigation of nonplanar dendronized polynuclear Ir complexes with subnanometer resolution using Ir as an atomic label. Decreasing the electron dose to the dendrimer complexes is critical for the single-molecule observation. A comparison with simulated STEM images of conformational isomers is performed to determine the most plausible conformation. Our results enlarge the potential of electron microscopic observation to realize structural analysis of coordination macromolecules, which has been impossible with conventional methods.

INTRODUCTION

Polynuclear coordination complexes have been studied intensively for decades because of their distinctive chemical and physical features and broad range of applications in material science (*1*–*14*). The key properties of metallo-macromolecules depend on their molecular structures, including both the local structures around metals and global orientation of peripheral ligand backbones. Hence, understanding relationships between structures and properties of metallo-macromolecules is essential for design of functional polynuclear coordination complexes. Despite their importance, structural analysis methods for polynuclear metal complexes are insufficient and still under development. The main difficulty arises from the limitations of conventional characterization techniques commonly used for small mononuclear coordination compounds. Apart from crystalline metal-organic framework families, it is generally difficult to obtain single crystals of polynuclear macromolecules with a suitable size for x-ray crystallography or electron diffractometry. Nuclear magnetic resonance (NMR) spectroscopy suffers from severe peak broadening and overlapping, with further complications in cases where paramagnetic metal ions are included. Fragmentation by dissociation of weak coordination bonds is a severe problem in mass spectrometry. As a result, metal atom arrangements in noncrystalline or amorphous coordination compounds have not been clarified, and research on this field is undeveloped. There is a strong demand for new analytical methods to determine the steric conformations of coordination macromolecules, which cannot be investigated by conventional analytical techniques.

Recently, microscopic observations have gained much attention for characterizing single molecules (*15*–*24*). Such microscopy can directly visualize real-time molecular structures with atomic resolution, providing not only structural but also dynamic information. In particular, atomically resolved high-angle annular dark-field scanning transmission electron microscopy (HAADF-STEM) can address the difficulty of characterizing coordination compounds with atomic resolution. The brightness of atom in HAADF-STEM images is theoretically almost quadratic of its atomic number (so-called *Z* contrast), which enables distinction of metal atoms from light organic backbone (*25*–*27*). Thus, HAADF-STEM allows direct determination of the metal atom positions and the numbers of overlapping atoms with their high contrast (*28*, *29*), which is impossible with conventional bright-field TEM observations. Positions of heavy metal atoms in coordination polymers definitely depend on the conformation of macromolecular backbone. In consequence, HAADF-STEM observation helps structural analysis of coordination compounds despite that it cannot directly resolve light elements such as C, N, and O. However, single-molecule observations of coordination compounds have still been limited to simple coordination complexes with low nuclearity less than 10 and planar or linear structures (*30*–*32*). Conventional staining method with OsO_4 or RuO_4 used for organic polymers is not suitable to atomic-resolution conformational analysis, owing to randomly occurred metal atom addition. Other atomic-resolution scanning probe microscopy techniques are neither useful for conformational analysis of nonplanar macromolecules. To the best of our knowledge, there has been no report on investigating polynuclear coordination molecules with complicated steric configurations to date.

Here, we describe the first conformational determination of polynuclear complexes with complicated steric structures, i.e., metallodendrimers, on the basis of HAADF-STEM images. Metallodendrimers have highly branched backbone, so that their precise conformational analysis related to their backbone and spatial arrangements of metal atoms have never been achieved in a single-molecule level. We have challenged the conformational analysis of invisible dendritic organic backbones using site–specifically metallated dendrimers. To make

[1]JST ERATO, Yamamoto Atom Hybrid Project, Tokyo Institute of Technology, 4259 Nagatsuta, Midori-ku, Yokohama 226-8503, Japan. [2]Institute of Innovative Research, Tokyo Institute of Technology, 4259 Nagatsuta, Midori-ku, Yokohama 226-8503, Japan.
*Corresponding author. Email: yamamoto.k.at@m.titech.ac.jp (K.Y.); imaoka.t.aa@m.titech.ac.jp (T.I.); albrecht@cm.kyushu-u.ac.jp (K.A.)
†Present address: Research Institute of Science and Technology, Tokyo University of Science, Chiba 278-8510, Japan.
‡Present address: Institute of Engineering Innovation, School of Engineering, The University of Tokyo, Tokyo 113-8656, Japan.
§Present address: Institute for Materials Chemistry and Engineering, Kyushu University, Fukuoka 816-8580, Japan.

the most of *Z* contrast in HAADF-STEM observations, we selected iridium (*Z* = 77) as a guide for conformational analysis. Our single-molecule structural investigation method via metal atom–guided HAADF-STEM image analysis successfully determined the conformations of a series of incremental polynuclear iridium complexes with dendritic phenylazomethine (DPA) ligands (fig. S1). The rigid backbone and stoichiometric coordination of DPAs are ideal for this model study (*33*, *34*). To achieve our goal, we performed rigid fixation of metal atoms to phenylazomethine moieties via cyclometallation reaction. Although the metallodendrimers were not stable under electron beam irradiation, we found that HAADF-STEM images obtained under low-damage conditions with a single scan reflected the original conformation of an individual complex molecule. Metal atoms in the complexes functioned as labels to determine their positions in the HAADF-STEM images, enabling the elucidation of the steric structure suitable for the HAADF-STEM images. This conformational analysis method is applicable to other coordination polymers/oligomers in principle, whereas further developments are necessary in practice. Therefore, our method will provide opportunities for conformation analysis of amorphous or noncrystalline coordination macromolecules at the single-molecule level guided by metal atom arrangement.

RESULTS

Cyclometallation of phenyazomethine with iridium(III)

We started the synthesis of a stable Ir complex with a phenylazomethine ligand using *N*,1,1-triphenylmethanimine (tpmi) as a model compound. We found that cyclometallation via carboxylate-assisted ortho C—H bond activation (*35*) efficiently gave the cycloiridated complex Cp*IrCl(tpmi) (Fig. 1A). The reaction of tpmi with $[Cp^*IrCl_2]_2$ (Cp*: $C_5(CH_3)_5$, pentamethylcyclopentadienyl) and sodium acetate in $CHCl_3$/CH_3OH afforded the half-sandwich–type cycloiridated complex in good yield. The ^{1}H-NMR spectrum of the reaction mixture indicated that the reaction occurs almost quantitatively.

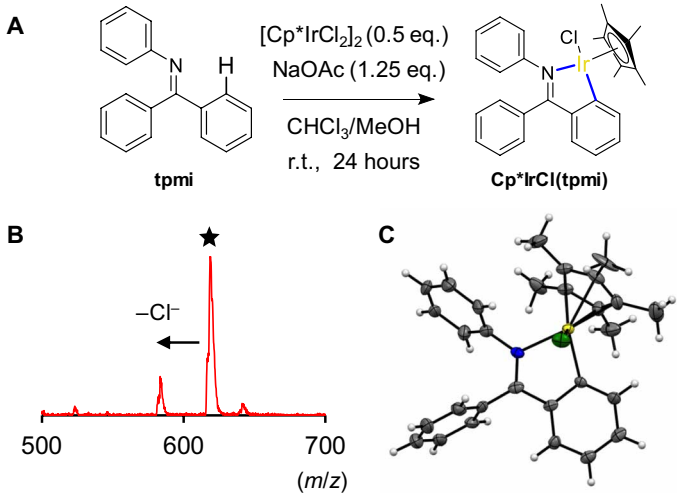

Fig. 1. Preparation and characterization of the mononuclear cycloiridated complex Cp*IrCl(tpmi). (**A**) Synthetic scheme for Cp*IrCl(tpmi). (**B**) MALDI-TOF-MS of Cp*IrCl(tpmi). (**C**) Single-crystal structure of Cp*IrCl(tpmi) with thermal ellipsoids at the 50% probability level. Yellow, Ir; green, Cl; blue, N; gray, C. MeOH, CH_3OH; eq., equivalents; r.t., room temperature; *m*/*z*, mass/charge ratio.

Cp*IrCl(tpmi) was fully characterized with conventional NMR spectroscopy, high-resolution mass spectrometry, and single-crystal x-ray structural analysis. The positive mode matrix-assisted laser desorption/ionization–time-of-flight mass spectrometry (MALDI-TOF-MS) in Fig. 1B features two peaks for the complex: the main peak for the radical cation of Cp*IrCl(tpmi) (marked with a star) and the subpeak for the chloride-dissociated cation, without fragments of dissociated phenylazomethine ligand. A single-crystal structural analysis of Cp*IrCl(tpmi) confirmed the formation of Ir—C(Ph) bond (Fig. 1C). The Ir—C(Ph) bond length was 2.049(8) Å, which is similar to those for previously reported cycloiridated phenylimines (*36*, *37*). The other bond lengths and angles are also reasonable for cycloiridated complexes. A space filling model with van der Waals radii shows that the bulky Cp* ring covers the Ir atom with interference from rotation of the phenyl group, causing peak broadening in the ^{1}H-NMR spectrum. Details of the synthesis and characterization are reported in the Supplementary Materials.

Complexation of DPAs with iridium

Fixation of iridium(III) in DPAs was achieved via carboxylate-assisted C—H bond activation (Fig. 2A). DPAs comprising 11 to 17 azomethine units were used, including newly synthesized dissymmetric dendrimers with 11, 13, 16, and 17 azomethines. These dissymmetric DPAs were synthesized by stepwise dehydration of 1,3,5-tris(4-aminophenyl)benzene with phenylazomethine dendrons (fig. S1, B and C). Addition of DPAs to a $[Cp^*IrCl_2]_2$ and sodium acetate mixture in tetrahydrofuran/CH_3OH efficiently afforded the corresponding iridium-decorated dendrimers $(Cp^*IrCl)_n$@*n*DPAs (*n* = 11 to 17; Fig. 2B). Reaction conditions such as stoichiometry of the Ir precursor, solvent polarity, and reaction time were modified from the model reaction for the mononuclear complex. The reaction was monitored by MALDI-TOF-MS, which indicated that the reaction was complete within 2 or 3 days. The positive-mode MALDI-TOF-MS of $(Cp^*IrCl)_n$@*n*DPAs features two main peaks, corresponding to the radical cation form and the Cl^--dissociated form. This means that the dissociation of Ir atoms from the dendrimer during mass spectrometry was negligible and that the determination of the number of Ir atoms bound to the dendrimer could be possible. The mass spectra indicated that the Ir species occupied all imine sites involving cycloiridation (Fig. 2C), indicating that DPAs have inner space enough to accommodate Cp*IrCl moieties. Metallodendrimers containing more iridium ions than imine sites were never detected. Therefore, the nuclarity of the Ir complexes was controllable by the number of the imine sites. The polynuclear iridium complexes were stable under ambient conditions for at least 4 months, such that the usual purification processes (e.g., extraction, column chromatography, and reprecipitation) were available to remove excess iridium precursors used in the reaction, affording the polynuclear complexes in good yields (60 to 70%). We note that the conventional characterization techniques were inadequate for the iridium complexes; usual ^{1}H-NMR spectra of the metallodendrimers were difficult to interpret because of severe broadening and overlapping of the signals (fig. S3), and single crystals of the iridated dendrimers were not obtained nor were those of the corresponding dendrimer ligands.

Atomic-resolution HAADF-STEM observation of Ir complexes

To check the atomicity of the Ir-containing dendrimers, we performed HAADF-STEM observations. HAADF-STEM is a powerful analytical method for the observation of heavy metal–containing

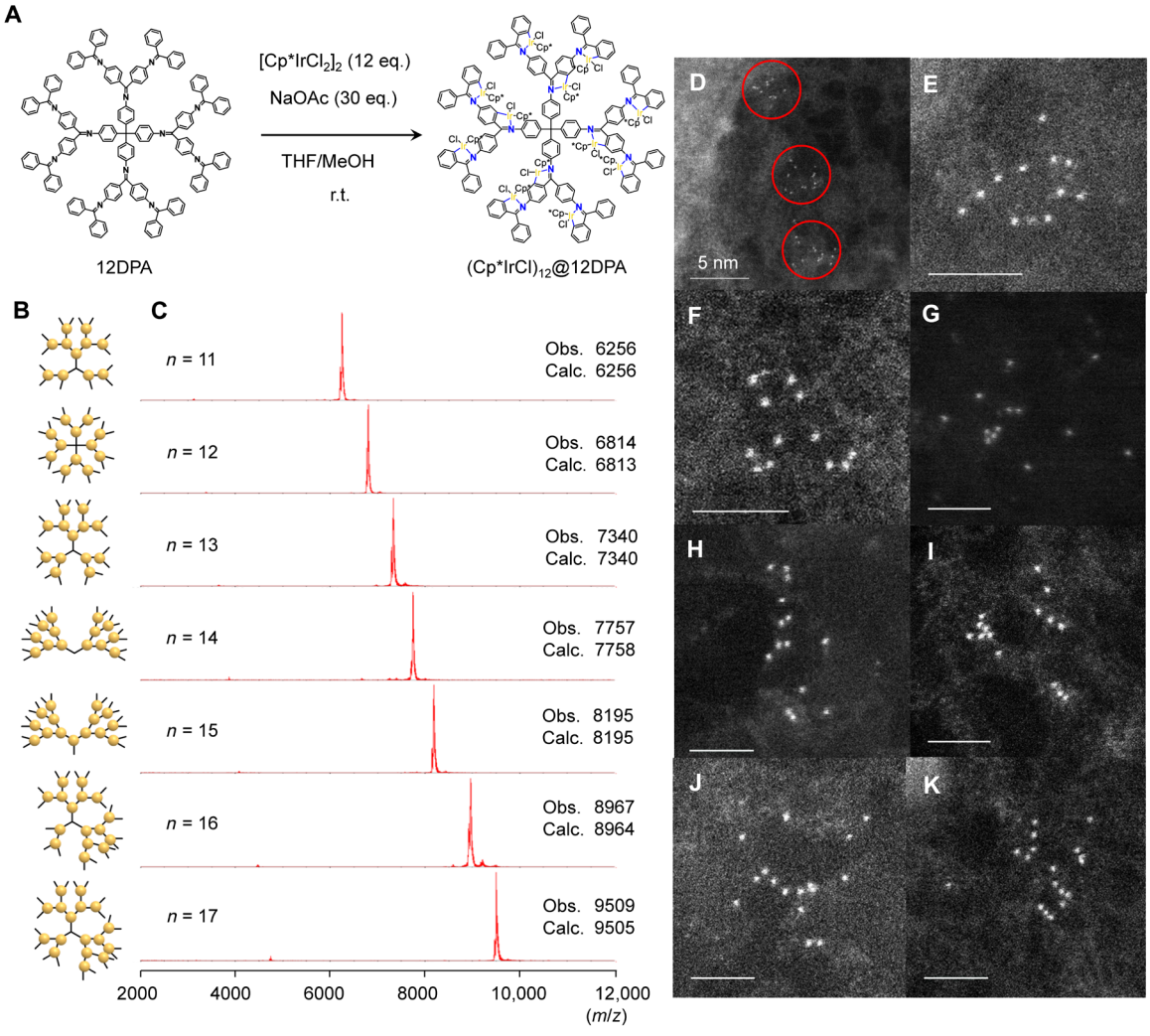

Fig. 2. Preparation and characterization of dendromized polynuclear Ir complexes (Cp*IrCl)$_n$@*n*DPA. (**A**) Synthetic scheme for (Cp*IrCl)$_n$@*n*DPA, represented by 12DPA. (**B**) Illustration of (Cp*IrCl)$_n$@*n*DPAs. (**C**) MALDI-TOF-MS of (Cp*IrCl)$_n$@*n*DPAs. (**D**) Low-magnification HAADF-STEM image of (Cp*IrCl)$_{12}$@12DPA on GNP. Individual complexes are marked with red circles. Scale bar, 5 nm. (**E** to **K**) Atom counting with atomic-resolution HAADF-STEM images of (Cp*IrCl)$_n$@*n*DPA. Scale bars, 2 nm.

compounds owing to the *Z* contrast. Various materials including nanostructured carbons and metal oxides can be used as a support for (Cp*IrCl)$_n$@*n*DPAs. For example, (Cp*IrCl)$_n$@*n*DPAs were adsorbed on graphene nanopowder (GNP) support by mixing a solution of the metallodendrimers and a suspension of GNP. Polar and poor solvents such as acetone and acetonitrile were suitable for immobilization of (Cp*IrCl)$_n$@*n*DPAs on the carbon support, whose surface is hydrophobic. To avoid dense immobilization of (Cp*IrCl)$_n$@*n*DPA on the surface, we set the mass loading of iridium below 0.1 weight % (wt %). (Cp*IrCl)$_n$@*n*DPAs on GNP were collected by filtration of the reaction mixture. The MALDI-TOF-MS spectrum of the colorless filtrate did not indicate the presence of Ir complexes, which implies almost quantitative adsorption of (Cp*IrCl)$_n$@*n*DPAs (fig. S4A). On the other hand, redispersion of the (Cp*IrCl)$_{12}$@12DPA-supporting GNP in chloroform promoted desorption of (Cp*IrCl)$_{12}$@12DPA from the surface, as seen in the MALDI-TOF-MS spectrum of the filtrate (fig. S4B) without dissociation of Ir from the dendrimers. Thus, (Cp*IrCl)$_n$@*n*DPAs were stable on the carbon support under ambient conditions.

HAADF-STEM images of (Cp*IrCl)$_n$@*n*DPAs dispersed on GNP demonstrated the precisely controlled atomicity of iridium. Figure 2D shows a HAADF-STEM image of (Cp*IrCl)$_{12}$@12DPA on GNP. In the image, each bright spot represents an iridium atom, and other light elements composing the complexes (e.g., C, H, and N) are hardly observable because of the low contrast on the GNP support. Other light elements such as S and Cl were present as contaminants on the GNPs and are observed as blurs or slightly bright spots. The positions of (Cp*IrCl)$_{12}$@12DPA are marked with red circles, showing that the metallodendrimers were well dispersed on the support. Low-magnification HAADF-STEM images of other (Cp*IrCl)$_n$@*n*DPAs are shown in fig. S4C. These complexes were also well dispersed on the GNP surface.

The atomic-resolution HAADF-STEM images of (Cp*IrCl)$_n$@*n*DPAs are shown in Fig. 2 (E to K). The number of bright spots directly reflects the number of iridium atoms in (Cp*IrCl)$_n$@*n*DPAs. In the images, iridium atoms are dispersed within a few square nanometers, and their numbers are equal to those of the imine sites of DPAs. Thus, the ensemble of iridium atoms corresponds to an

individual polynuclear complex. These atomic-resolution observations require a certain time to adjust the focus. Thus, the atomic-resolution observation described here leads to the decomposition of $(Cp^*IrCl)_n$@*n*DPAs by electron beam irradiation despite the low accelerating voltage of 80 kV. Ensembles of Ir atoms are also observable on other supports such as ketjenblack and magnesium oxide nanopowder, highlighting the individual Ir complexes (fig. S5). Some of the Ir complexes partially lost Ir atoms during focus adjustment, leading to fewer Ir atoms in the observed images.

Metal atom–guided conformational analysis of polynuclear Ir complexes

For conformational elucidation of single $(Cp^*IrCl)_n$@*n*DPA molecules, HAADF-STEM observations with reduced damage to the molecules were performed. As mentioned, STEM observations using the low acceleration voltage of 80 kV were still insufficient to prevent the decomposition of the Ir complexes. Further reducing the electron dose and exposure time was expected to keep the complex for a certain time, thus enabling conformational analysis using the positions of metal atoms as structure labels. To achieve the conformational analysis of $(Cp^*IrCl)_n$@*n*DPAs on GNP, we performed atomic-resolution HAADF-STEM observations of the complexes under damage-reducing conditions. The beam current was reduced from 26 to 7 pA. The exposure time per pixel was set to 8 μs, and observations were performed at low magnification to reduce the exposure time for each molecule. In addition, a single scan of an area was used to obtain the image after adjusting the focus for a neighboring area (Fig. 3A). These conditions reduced the energy that the complexes accepted from the electron beam. Figure 3B shows a HAADF-STEM image of $(Cp^*IrCl)_{12}$@12DPA obtained under these low-damage conditions. Although the image is less clear than the images taken under the usual conditions (Fig. 2D), it is enough to determine the positions of Ir atoms. Compared to the image obtained under the usual conditions, the Ir atoms are distributed over a narrow area, implying reduced damage to the molecules. Using the same conditions, HAADF-STEM images of $(Cp^*IrCl)_n$@*n*DPAs were collected (fig. S6). Although HAADF-STEM can distinguish overlapping of heavy metal atoms by contrast in images, STEM images without overlapping Ir atoms were better for conformational analysis. Thus, STEM images of individual molecules in fig. S6 were then subjected to conformational analysis.

Conformational analysis of Ir complexes was performed with the aid of simulated STEM images drawn by a BioNet elbis software, which can simulate both TEM and STEM images of single molecules. A schematic illustration of the conformational analysis process is shown in Fig. 4. To identify the molecular structure using the experimental STEM images, we generated conformational isomers of $(Cp^*IrCl)_n$@*n*DPA at first. These conformational isomers have simplified structures with the replacement of Cp* with Cp (Cp: C_5H_5, cyclopentadienyl). This replacement has no substantial influence on the STEM simulation because of the low contrast of C and H, but the less sterically hindered structure enables a wider conformational scope. The conformational isomers were produced from a semiempirically optimized structure by randomly rotating C—N single bonds except for those of the most peripheral imines, because their rotation had little influence on the positions of Ir atoms. For example, $(Cp^*IrCl)_{12}$@12DPA is a second-generation metallodendrimer, comprising four inner-layer imines and eight outer-layer imines. The rotation of four C—N single bonds in the inner-layer imines is more dominant in the STEM simulation, because their rotation causes a large displacement of 0.8 nm in the outer-layer Ir atoms. On the other hand, the rotation of the outer layer imine sites causes a small displacement of about 0.2 nm to the outer-layer Ir and no displacement to the inner-layer Ir (fig. S7). The dihedral angles of the rotatable C—N single bonds were randomly selected from −180° to 180°. Considering that small differences in the dihedral angles did not substantially influence the simulated image, 20 to 30 conformers were enough to search plausible structure in this simplified method. The produced conformers included sterically hindered structures, which were excluded. Ten to 15 isomers satisfied the steric demand at this stage. The allowed structures were subjected to TEM simulations where only iridium atoms were considered, to find the most plausible orientation for each conformer. The removal of the other elements gave simulated TEM images similar to simulated STEM images with lower calculation costs and times. The matching program based on a Radon transform implemented in the software provided a suitable candidate for the conformers and their orientation. The structure of the candidate conformers was again refined by modifying bond lengths, angles, and dihedral angles around all C—N single bonds. Last, Cp ligands were transformed back to Cp*, and the rotation of Cp* rings, methyl groups, and phenylene groups of the dendrimer backbone was adjusted to

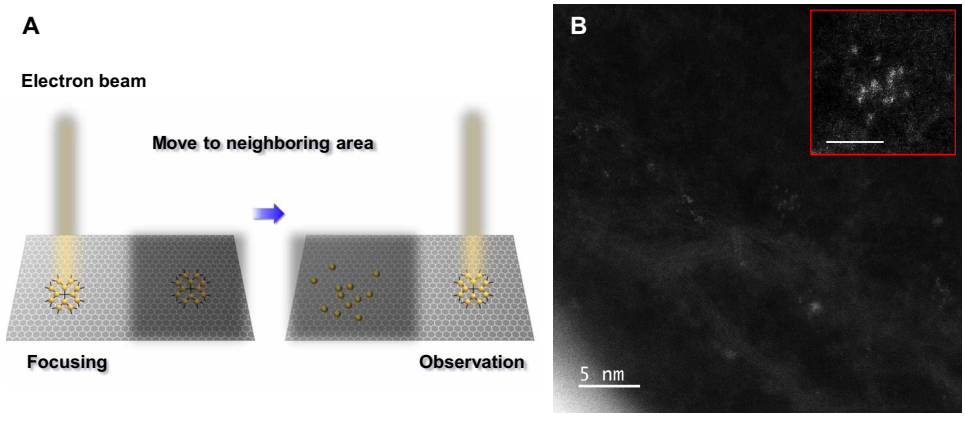

Fig. 3. Low-damage HAADF-STEM observation of the polynuclear Ir complexes. (**A**) Schematic illustration of low-damage HAADF-STEM observation. (**B**) HAADF-STEM image of $(Cp^*IrCl)_{12}$@12DPA on GNP obtained with the low-damage method. Inset: Magnified with atomic resolution. Scale bar, 2 nm.

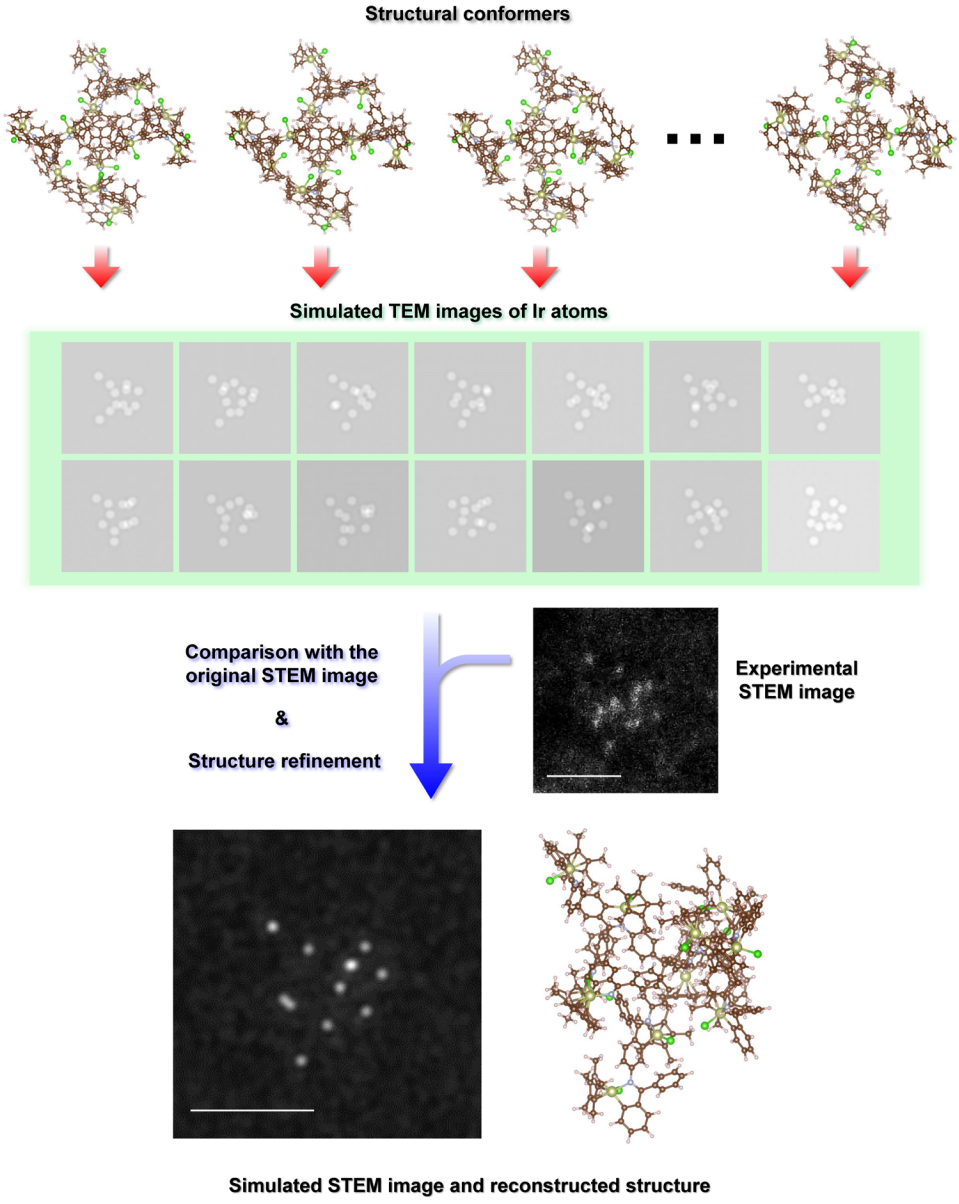

Fig. 4. Schematic illustration of atom-guided structural elucidation of $(Cp^*IrCl)_n$@*n*DPA. Structural analysis method for $(Cp^*IrCl)_{12}$@12DPA was shown as an example. The clarified structure and corresponding simulated STEM images were demonstrated at the bottom. Scale bar, 2 nm for both experimental and simulated images.

reduce steric repulsion with the bulky Cp* group. The double-step conformation analysis enables the discovery of the most plausible conformers from relatively small numbers of conformer candidates. We note that, in this study, both the rigid molecular structure of DPA by π-conjugation and the number of Ir atoms from 11 to 17 contribute to the reduction of calculation cost and enables conformation analysis with the simplified method. The obtained structure was subjected to single-point energy calculation at the semiempirical pm6 level of theory to check the steric validity.

The analysis of HAADF-STEM images could reproduce the conformations of $(Cp^*IrCl)_{12}$@12DPA. As shown in the bottom of Fig. 4, the experimental HAADF-STEM image was well fitted by the simulated image. To evaluate the validity of the obtained structure, we introduced the mean difference between the positions of the observed and simulated Ir atoms, annotated as Δd (defined by Eq. 1 in Materials and Methods). For $(Cp^*IrCl)_{12}$@12DPA, Δd value was 0.25 ± 0.13 nm. This value is comparable to the diameter of an iridium atom (0.27 nm) (*38*) and the displacement caused by C—N bond free rotation (0.2 nm). Thus, we conclude that the conformation of the polynuclear complex was well determined. Owing to the steric demand by highly hindered structure of $(Cp^*IrCl)_{12}$@12DPA, the reproduced structure seemed the most plausible conformation for the complex. Errors can be attributed to the dynamic motion of the molecules, such as partial rotation of single bonds and bending of the molecule, and sample drift during the acquisition of the images.

All polynuclear Ir complexes were sterically resolved by our method. Figure 5 summarizes the structural fitting results for Ir

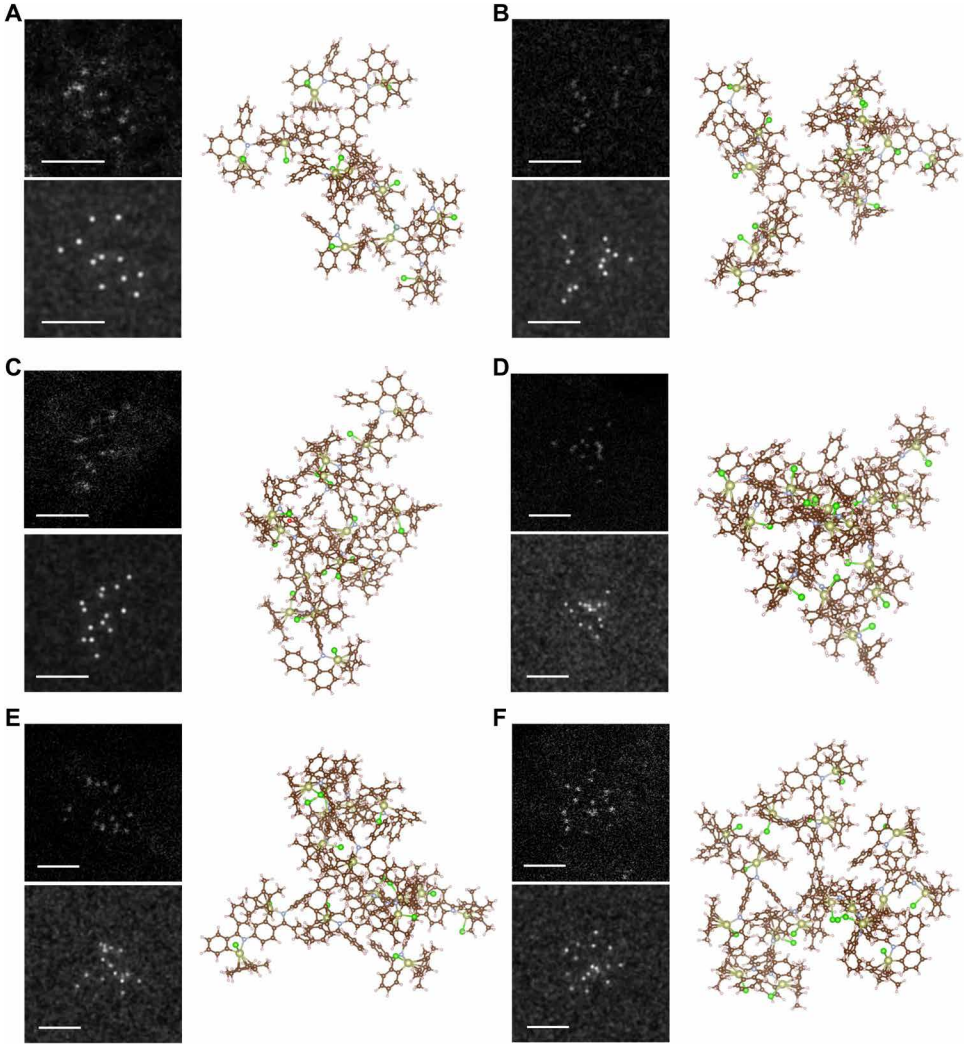

Fig. 5. Metal atom-guided conformational analysis via HAADF-STEM observations. Atomically resolved HAADF-STEM images (top left), simulated HAADF-STEM images of $(Cp^*IrCl)_n$@*n*DPAs [*n* = 11, 13, 14, 15, 16, and 17 for (**A**), (**B**), (**C**), (**D**), (**E**), and (**F**), respectively] on GNP obtained with the low-damage method (bottom left), and conformation and orientation of the Ir complexes corresponding to the simulated images (right). Scale bars, 2 nm.

complexes. The experimental HAADF-STEM images are shown on the top left, and the simulated images are at the bottom left. On the right side, the molecular structures of $(Cp^*IrCl)_n$@*n*DPAs were shown with the conformation and orientation for the STEM simulation. Δd values for $(Cp^*IrCl)_n$@*n*DPAs are 0.35 ± 0.18 (*n* = 11), 0.25 ± 0.13 (*n* = 12), 0.24 ± 0.18 (*n* = 13), 0.25 ± 0.12 (*n* = 14), 0.27 ± 0.17 (*n* = 15), 0.40 ± 0.20 (*n* = 16), and 0.23 ± 0.16 (*n* = 17). The 12-, 13-, 14-, 15-, and 17-nuclear complexes showed good agreement between the experimental and simulated images, while there were the moderate Δd values for 11- and 16-nuclear complexes. Although the simulated and experimental images are not perfectly identical, the errors of ca. 0.2 to 0.3 nm are reasonable for HAADF-STEM observation of coordination compounds (*30*, *31*). Because of the adsorption on the support, the bond angles and distances were not those for theoretically predicted stable structures in vacuum, which is typical for surface confined species. For all complexes, single-point energy calculations at semiempirical pm6 level were completed without any error stemming from steric problems. Thus, the reproduced structures of the iridium complexes are sterically possible. The detailed structures of the complexes with the space-filling models based on van der Waals radii are shown in fig. S8. These models demonstrate densely packed structures for the Ir complexes. In these structures, we could see that some terminal of dendron was located nearby the core moiety, the so-called back-folding. This phenomenon was not observed by the previous reports of DPAs on the basis of gel-permeation chromatography analysis (*39*) and first observed by the analysis in the single-molecule level. For example, in the case of $(Cp^*IrCl)_{17}$@17DPA, the distance between a core C atom and one terminal C atom was 6.6 Å, which was shorter than the distance between the core C atom and the inner Ir atom (7.0 Å). The bulky Cp* groups in the metallodendrimers are attributable to the back-folding by the hydrophobic interactions of dendrons. Because of the back-folding, the rotation of phenyl groups and conformational transformation via C—N single bonds were limited by steric hindrance between the dendrons, especially those nearest to the core of the metallodendrimers. This steric locking and high steric hindrance makes NMR measurement difficult.

DISCUSSION

In summary, we have established an unprecedented conformational analysis method for single polynuclear coordination mocromolecules guided by metal atoms with atomic-resolution HAADF-STEM observations at room temperature. The heavy metal atoms function as atomic labels, guiding assignment of steric conformations of organic backbones in polynuclear complexes. Conformational analysis of a series of polynuclear Ir complexes with DPA ligands demonstrated the utility of this method to produce snapshots of polynuclear coordination compounds. Our study here is a pioneering example to investigate steric structures of noncrystalline polynuclear coordination compounds by atomic-resolution microscopy. In principle, STEM simulations for all conformers and orientations and quantitative investigation of degree of matching between simulated and experimental images can find the most plausible conformation for any coordination compounds except enantiomers. Development of better observation methods for obtaining clear images enough to carry out conformational analysis in depth and more efficient analytic algorithms to reconstruct molecular structures from experimental images will enhance usefulness of our conformational analysis method. For further study, metal atom–guided conformational analysis of a multinuclear metallopeptide with more flexible structure is under way. We believe that our discovery will lead to the further development for conformational elucidation of polynuclear coordination compounds by atomically resolved electron microscopy.

MATERIALS AND METHODS

Materials

12DPA, 14DPA, and 15DPA were synthesized according to previously reported procedures (*39*–*41*). The preparation of other *n*DPAs is described in the Supplementary Materials. $[Cp^*IrCl_2]_2$ and sodium acetate were purchased from Kanto Chemical Co. Ltd. and used without further purification. All the anhydrous solvents were purchased from Kanto Chemical Co. Ltd. GNP (1.6-nm thickness) was purchased from Alliance Biosystems Inc. Ketjenblack EC600JD was obtained from Lion Specialty Chemicals Co. Ltd. MgO nanopowder was purchased from Sigma-Aldrich Co. LLC.

Apparatus

MALDI-TOF-MS spectra were collected using Shimadzu AXIMA CFR-plus and Bruker microflex-YI mass spectrometers. Dithranol and *trans*-2-[3-(4-*tert*-Butylphenyl)-2-methyl-2-propenylidene]malononitrile (DCTB, Tokyo Chemical Industry Co. Ltd.) were used as matrices. HAADF-STEM images were obtained with a JEOL ARM200F electron microscope at 80 kV. The Ir complexes immobilized on GNP were suspended in MeOH and then dropped onto carbon microgrid–decorated Cu grids (Nisshin EM Co. Ltd.). The decorated TEM grids were dried and stored under vacuum. STEM simulations were performed using BioNet elbis software (BioNet Laboratory Inc.). An amorphous carbon layer was embedded below the Ir to reproduce the observed STEM images.

Preparation of $(Cp^*IrCl)_{12}$@12DPAs

Under an Ar atmosphere, 12DPA (2 mg/ml in THF/MeOH = 1/1) was added to a THF/MeOH suspension of $[Cp^*IrCl_2]_2$ and NaOAc (1.0 and 2.5 equivalent to total imine sites, respectively). The mixture was stirred until reaction completion, followed by the removal of the solvent under reduced pressure. The residue was dissolved in $CHCl_3$, and insoluble by-products were removed by filtration. The crude product was purified by silica gel column chromatography (eluent, $CHCl_3$) and reprecipitation from $CHCl_3$/MeOH. The other $(Cp^*IrCl)_n$@*n*DPAs were prepared by the same procedure using the appropriate *n*DPA.

Immobilization of Ir complexes on supports

GNP was suspended in acetone (0.5 mg/ml) by ultrasonication for 3 hours. To the suspension, an acetone solution of $(Cp^*IrCl)_n$@*n*DPA (0.2 μM) was added until the Ir loading reached 0.1 wt %, and the mixture was further sonicated to 1 hour. $(Cp^*IrCl)_n$@*n*DPA on GNP was collected by filtration and dried under vacuum. The obtained black powder was used for STEM observation. Immobilization on ketjenblack was performed by the same method, while toluene was used instead of acetone for immobilization on MgO nanopowder.

Modeling of Ir complexes

The model structures of the Ir complexes were created by the following steps. First, simplified model structures, where Cp* groups were replaced with Cp groups, were created using the GaussView 6 package, and structural optimization was the performed by the semiempirical pm6 calculation method (*42*) using the Gaussian 16 package (*43*). The dihedral angles of rotatable C─N single bonds except for the most peripheral imine sites were randomly changed to create conformational isomers. After the exclusion of sterically prohibited structures, TEM image simulation for the complexes where only Ir atoms were considered was performed. Plausible conformers were selected by comparison of the observed STEM image and the simulated TEM images via a one-dimensional matching program in the BioNet elbis software. The plausible structures were further refined by manual adjusting bond angles, dihedral angles, and bond lengths to reduce the mean difference between observed and simulated positions of Ir atoms. Last, the hydrogens in the Cp rings were replaced with CH_3 groups to convert them into Cp* rings, and steric repulsion was reduced by rotating Cp* rings, free-rotating Ph groups, and C─N single bonds. The simulated STEM images were evaluated on the basis of the mean difference between the positions of observed and simulated Ir atoms, Δd, defined as follows

$$\Delta d = \frac{1}{n}\sum\sqrt{(x_{ok} - x_{sk})^2 + (y_{ok} - y_{sk})^2} \quad (1)$$

where x_{ok} and y_{ok} are the observed coordinates of Ir atoms, x_{sk} and y_{sk} are the simulated coordinates of Ir atoms, and n is the number of Ir atoms. For both observed and simulated images, the origin is located at the center of gravity of the iridium atoms.

SUPPLEMENTARY MATERIALS

Supplementary material for this article is available at http://advances.sciencemag.org/cgi/content/full/7/32/eabd9887/DC1

REFERENCES AND NOTES

1. A. Winter, U. S. Schubert, Synthesis and characterization of metallo-supramolecular polymers. *Chem. Soc. Rev.* **45**, 5311–5357 (2016).
2. Y. Wang, D. Astruc, A. S. Abd-El-Aziz, Metallopolymers for advanced sustainable applications. *Chem. Soc. Rev.* **48**, 558–636 (2019).
3. K. C. Bentz, S. M. Cohen, Supramolecular metallopolymers: From linear materials to infinite networks. *Angew. Chem. Int. Ed.* **57**, 14992–15001 (2018).
4. P.-L. Wang, L.-H. Xie, E. A. Joseph, J.-R. Li, X.-O. Su, H.-C. Zhou, Metal–organic frameworks for food safety. *Chem. Rev.* **119**, 10638–10690 (2019).

5. K. J. Waldron, J. C. Rutherford, D. Ford, N. J. Robinson, Metalloproteins and metal sensing. *Nature* **460**, 823–830 (2009).
6. L. Ren, J. Lv, H. Wang, Y. Cheng, A coordinative dendrimer achieves excellent efficiency in cytosolic protein and peptide delivery. *Angew. Chem. Int. Ed.* **59**, 4711–4719 (2020).
7. R. Toyoda, R. Sakamoto, N. Fukui, R. Matsuoka, M. Tsuchiya, H. Nishihara, A single-stranded coordination copolymer affords heterostructure observation and photoluminescence intensification. *Sci. Adv.* **5**, eaau0637 (2019).
8. C. Lochenie, K. Schötz, F. Panzer, H. Kurz, B. Maier, F. Puchtler, S. Agarwal, A. Köhler, B. Weber, Spin-crossover iron(II) coordination polymer with fluorescent properties: Correlation between emission properties and spin state. *J. Am. Chem. Soc.* **140**, 700–709 (2018).
9. Y. Liu, C. C. L. McCrory, Modulating the mechanism of electrocatalytic CO_2 reduction by cobalt phthalocyanine through polymer coordination and encapsulation. *Nat. Commun.* **10**, 1683 (2019).
10. K. Wada, K. Sakaushi, S. Sasaki, H. Nishihara, Multielectron-transfer-based rechargeable energy storage of two-dimensional coordination frameworks with non-innocent ligands. *Angew. Chem. Int. Ed.* **57**, 8886–8890 (2018).
11. W. Li, F. Li, H. Yang, X. Wu, P. Zhang, Y. Shan, L. Sun, A bio-inspired coordination polymer as outstanding water oxidation catalyst via second coordination sphere engineering. *Nat. Commun.* **10**, 5074 (2019).
12. M. Shivanna, Q.-Y. Yang, A. Bajpai, S. Sen, N. Hosono, S. Kusaka, T. Pham, K. A. Forrest, B. Space, S. Kitagawa, M. J. Zaworotko, Readily accessible shape-memory effect in a porous interpenetrated coordination network. *Sci. Adv.* **4**, eaaq1636 (2018).
13. Q. Chen, A. Dong, D. Wang, L. Qiu, C. Ma, Y. Yuan, Y. Zhao, N. Jia, Z. Guo, N. Wang, Efficient and selective methane borylation through pore size tuning of hybrid porous organic-polymer-based iridium catalysts. *Angew. Chem. Int. Ed.* **58**, 10671–10676 (2019).
14. L. J. A. Macedo, A. Hassan, G. C. Sedenho, F. N. Crespilho, Assessing electron transfer reactions and catalysis in multicopper oxidases with operando X-ray absorption spectroscopy. *Nat. Commun.* **11**, 316 (2020).
15. G. Binnig, H. Rohrer, C. Gerber, E. Weibel, Surface studies by scanning tunneling microscopy. *Phys. Rev. Lett.* **49**, 57–61 (1982).
16. Z. Zhang, Y. Li, B. Song, Y. Zhang, X. Jiang, M. Wang, R. Tumbleson, C. Liu, P. Wang, X.-Q. Hao, T. Rojas, A. T. Ngo, J. L. Sessler, G. R. Newkome, S. W. Hla, X. Li, Intra- and intermolecular self-assembly of a 20-nm-wide supramolecular hexagonal grid. *Nat. Chem.* **12**, 468–474 (2020).
17. L. Gross, F. Mohn, N. Moll, P. Liljeroth, G. Meyer, The chemical structure of a molecule resolved by atomic force microscopy. *Science* **325**, 1110–1114 (2009).
18. K. Kaiser, L. M. Scriven, F. Schulz, P. Gawel, L. Gross, H. L. Anderson, An sp-hybridized molecular carbon allotrope, cyclo[18]carbon. *Science* **365**, 1299–1301 (2019).
19. M. Koshino, T. Tanaka, N. Solin, K. Suenaga, H. Isobe, E. Nakamura, Imaging of single organic molecules in motion. *Science* **316**, 853 (2007).
20. E. Nakamura, M. Koshino, T. Saito, Y. Niimi, K. Suenaga, Y. Matsuo, Electron microscopic imaging of a single group 8 metal atom catalyzing C-C bond reorganization of fullerenes. *J. Am. Chem. Soc.* **133**, 14151–14153 (2011).
21. S. Okada, S. Kowashi, L. Schweighauser, K. Yamanouchi, K. Harano, E. Nakamura, Direct microscopic analysis of individual C_{60} dimerization events: Kinetics and mechanisms. *J. Am. Chem. Soc.* **139**, 18281–18287 (2017).
22. J. Xing, L. Schweighauser, S. Okada, K. Harano, E. Nakamura, Atomistic structures and dynamics of prenucleation clusters in MOF-2 and MOF-5 syntheses. *Nat. Commun.* **10**, 3608 (2019).
23. T. Nakamuro, M. Sakakibara, H. Nada, K. Harano, E. Nakamura, Capturing the moment of emergence of crystal nucleus from disorder. *J. Am. Chem. Soc.* **143**, 1763–1767 (2021).
24. E. Nakamura, Atomic-resolution transmission electron microscopic movies for study of organic molecules, assemblies, and reactions: The first 10 years of development. *Acc. Chem. Res.* **50**, 1281–1292 (2017).
25. P. Hartel, H. Rose, C. Dinges, Conditions and reasons for incoherent imaging in STEM. *Ultramicroscopy* **63**, 93–114 (1996).
26. O. L. Krivanek, M. F. Chisholm, V. Nicolosi, T. J. Pennycook, G. J. Corbin, N. Dellby, M. F. Murfitt, C. S. Own, Z. S. Szilagyi, M. P. Oxley, S. T. Pantelides, S. J. Pennycook, Atom-by-atom structural and chemical analysis by annular dark-field electron microscopy. *Nature* **464**, 571–574 (2010).
27. S. Yamashita, J. Kikkawa, K. Yanagisawa, T. Nagai, K. Ishizuka, K. Kimoto, Atomic number dependence of *Z* contrast in scanning transmission electron microscopy. *Sci. Rep.* **8**, 12325 (2018).
28. T. Imaoka, T. Toyonaga, M. Morita, N. Haruta, K. Yamamoto, Isomerizations of a Pt_4 cluster revealed by spatiotemporal microscopic analysis. *Chem. Commun.* **55**, 4753–4756 (2019).
29. H. Yasumatsu, T. Tohei, Y. Ikuhara, Determination of exact positions of individual tungsten atoms in unisize tungsten oxide clusters supported on carbon substrate by HAADF-STEM observation. *J. Phys. Chem. C* **118**, 1706–1711 (2014).
30. M. A. Gerkman, S. Sinha, J. H. Warner, G. G. D. Han, Direct imaging of photoswitching molecular conformations using individual metal atom markers. *ACS Nano* **13**, 87–96 (2019).
31. J. K. Lee, I. Bulut, M. Rickhaus, Y. Sheng, X. Li, G. G. D. Han, G. A. D. Briggs, H. L. Anderson, J. H. Warner, Metal atom markers for imaging epitaxial molecular self-assembly on graphene by scanning transmission electron microscopy. *ACS Nano* **13**, 7252–7260 (2019).
32. M. A. Gerkman, J. K. Lee, X. Li, Q. Zhang, M. Windley, M. V. Fonseca, Y. Lu, J. H. Warner, G. G. D. Han, Direct imaging of individual molecular binding to clean nanopore edges in 2D monolayer MoS_2. *ACS Nono* **14**, 153–165 (2020).
33. K. Yamamoto, M. Higuchi, S. Shiki, M. Tsuruta, H. Chiba, Stepwise radial complexation of imine groups in phenylazomethine dendrimers. *Nature* **415**, 509–511 (2002).
34. T. Tsukamoto, T. Kambe, A. Nakao, T. Imaoka, K. Yamamoto, Atom-hybridization for synthesis of polymetallic clusters. *Nat. Commun.* **9**, 3873 (2018).
35. L. Ackermann, Carboxylate-assisted transition-metal-catalyzed C-H bond functionalizations: Mechanism and scope. *Chem. Rev.* **111**, 1315–1345 (2011).
36. D. L. Davies, O. Al-Duaij, J. Fawcett, M. Giardiello, S. T. Hilton, D. R. Russell, Room-temperature cyclometallation of amines, imines and oxazolines with $[MCl_2Cp^*]_2$ (M = Rh, Ir) and $[RuCl_2(p\text{-cymene})]_2$. *Dalton Trans.* **2003**, 4132–4138 (2003).
37. L. Li, W. W. Brennessel, W. D. Jones, An efficient low-temperature route to polycyclic isoquinoline salt synthesis via C–H activation with $[Cp^*MCl_2]_2$ (M = Rh, Ir). *J. Am. Chem. Soc.* **130**, 12414–12419 (2008).
38. J. C. Slator, Atomic radii in crystals. *J. Chem. Phys.* **41**, 3199–3204 (1964).
39. O. Enoki, H. Katoh, K. Yamamoto, Synthesis and properties of a novel phenylazomethine dendrimer with a tetraphenylmethane core. *Org. Let.* **8**, 569–571 (2006).
40. K. Yamamoto, M. Higuchi, A. Kimoto, T. Imaoka, K. Masachika, Novel functional groups with fine-controlled metal assembling function. *Bull. Chem. Soc. Jpn.* **78**, 349–355 (2005).
41. M. Higuchi, S. Shiki, K. Yamamoto, Novel phenylazomethine dendrimers: Synthesis and structural properties. *Org. Lett.* **2**, 3079–3082 (2000).
42. J. J. P. Stewart, Optimization of parameters for semiempirical methods V: Modification of NDDO approximations and application to 70 elements. *J. Mol. Model.* **13**, 1173–1213 (2007).
43. M. J. Frisch, G. W. Trucks, H. B. Schlegel, G. E. Scuseria, M. A. Robb, J. R. Cheeseman, G. Scalmani, V. Barone, G. A. Petersson, H. Nakatsuji, X. Li, M. Caricato, A. V. Marenich, J. Bloino, B. G. Janesko, R. Gomperts, B. Mennucci, H. P. Hratchian, J. V. Ortiz, A. F. Izmaylov, J. L. Sonnenberg, D. Williams-Young, F. Ding, F. Lipparini, F. Egidi, J. Goings, B. Peng, A. Petrone, T. Henderson, D. Ranasinghe, V. G. Zakrzewski, J. Gao, N. Rega, G. Zheng, W. Liang, M. Hada, M. Ehara, K. Toyota, R. Fukuda, J. Hasegawa, M. Ishida, T. Nakajima, Y. Honda, O. Kitao, H. Nakai, T. Vreven, K. Throssell, J. A. Montgomery, Jr., J. E. Peralta, F. Ogliaro, M. J. Bearpark, J. J. Heyd, E. N. Brothers, K. N. Kudin, V. N. Staroverov, T. A. Keith, R. Kobayashi, J. Normand, K. Raghavachari, A. P. Rendell, J. C. Burant, S. S. Iyengar, J. Tomasi, M. Cossi, J. M. Millam, M. Klene, C. Adamo, R. Cammi, J. W. Ochterski, R. L. Martin, K. Morokuma, O. Farkas, J. B. Foresman, and D. J. Fox, Gaussian 16, Revision A.03 (Gaussian Inc., 2016).
44. G. M. Sheldrick, *SHELXT* – Integrating space group determination and structure solution. *Acta Crystallogr.* **71**, 1–8 (2015).

Acknowledgments: We are grateful to T. Liang for the synthesis of DPAs and Y. Hayashi for the HAADF-STEM observations. We also thank colleagues in the Suzukakedai Materials Analysis Division, Technical Department, Tokyo Institute of Technology, for elemental analysis. **Funding:** This study was supported by JST ERATO, Japan, grant no. JPMJER1503 (K.Y.) and Grant-in-Aid for Early-Career Scientists, KAKENHI nos. 18 K14072 and 20 K15242 (K.T.). **Author contributions:** K.T. carried out the synthesis and characterization of Ir complexes, the collection of the HAADF-STEM images, and the structural investigation from the HAADF-STEM images. M.M. conducted the HAADF-STEM observations. K.A. promoted the synthesis of the dendrimer ligands with J.K. K.T., T.I., and K.Y. wrote the manuscript. T.I. and K.Y. supervised the current study. K.Y. was the project leader for this study. **Competing interests:** The authors declare that they have no competing interests. **Data and materials availability:** All data needed to evaluate the conclusions in the paper are present in the paper and/or the Supplementary Materials. Additional data related to this paper may be requested from the authors.

Submitted 24 July 2020
Accepted 21 June 2021
Published 6 August 2021
10.1126/sciadv.abd9887

Citation: K. Takada, M. Morita, T. Imaoka, J. Kakinuma, K. Albrecht, K. Yamamoto, Metal atom–guided conformational analysis of single polynuclear coordination molecules. *Sci. Adv.* **7**, eabd9887 (2021).